

Measurement of the form factors of the decay $B^0 \rightarrow D^{*-} \ell^+ \nu_\ell$ and determination of the CKM matrix element $|V_{cb}|$

I. Adachi,¹⁰ H. Aihara,⁵¹ D. Anipko,¹ K. Arinstein,¹ T. Aso,⁵⁵ V. Aulchenko,¹
 T. Aushev,^{22,16} T. Aziz,⁴⁷ S. Bahinipati,³ A. M. Bakich,⁴⁶ V. Balagura,¹⁶ Y. Ban,³⁸
 E. Barberio,²⁵ A. Bay,²² I. Bedny,¹ K. Belous,¹⁵ V. Bhardwaj,³⁷ U. Bitenc,¹⁷ S. Blyth,²⁹
 A. Bondar,¹ A. Bozek,³¹ M. Bračko,^{24,17} J. Brodzicka,^{10,31} T. E. Browder,⁹ M.-C. Chang,⁴
 P. Chang,³⁰ Y.-W. Chang,³⁰ Y. Chao,³⁰ A. Chen,²⁸ K.-F. Chen,³⁰ B. G. Cheon,⁸
 C.-C. Chiang,³⁰ R. Chistov,¹⁶ I.-S. Cho,⁵⁷ S.-K. Choi,⁷ Y. Choi,⁴⁵ Y. K. Choi,⁴⁵ S. Cole,⁴⁶
 J. Dalseno,¹⁰ M. Danilov,¹⁶ A. Das,⁴⁷ M. Dash,⁵⁶ A. Drutskoy,³ W. Dungel,¹⁴ S. Eidelman,¹
 D. Epifanov,¹ S. Esen,³ S. Fratina,¹⁷ H. Fujii,¹⁰ M. Fujikawa,²⁷ N. Gabyshev,¹
 A. Garmash,³⁹ P. Goldenzweig,³ B. Golob,^{23,17} M. Grosse Perdekamp,^{12,40} H. Guler,⁹
 H. Guo,⁴² H. Ha,¹⁹ J. Haba,¹⁰ K. Hara,²⁶ T. Hara,³⁶ Y. Hasegawa,⁴⁴ N. C. Hastings,⁵¹
 K. Hayasaka,²⁶ H. Hayashii,²⁷ M. Hazumi,¹⁰ D. Heffernan,³⁶ T. Higuchi,¹⁰ H. Hödlmoser,⁹
 T. Hokuue,²⁶ Y. Horii,⁵⁰ Y. Hoshi,⁴⁹ K. Hoshina,⁵⁴ W.-S. Hou,³⁰ Y. B. Hsiung,³⁰
 H. J. Hyun,²¹ Y. Igarashi,¹⁰ T. Iijima,²⁶ K. Ikado,²⁶ K. Inami,²⁶ A. Ishikawa,⁴¹ H. Ishino,⁵²
 R. Itoh,¹⁰ M. Iwabuchi,⁶ M. Iwasaki,⁵¹ Y. Iwasaki,¹⁰ C. Jacoby,²² N. J. Joshi,⁴⁷ M. Kaga,²⁶
 D. H. Kah,²¹ H. Kaji,²⁶ H. Kakuno,⁵¹ J. H. Kang,⁵⁷ P. Kapusta,³¹ S. U. Kataoka,²⁷
 N. Katayama,¹⁰ H. Kawai,² T. Kawasaki,³³ A. Kibayashi,¹⁰ H. Kichimi,¹⁰ H. J. Kim,²¹
 H. O. Kim,²¹ J. H. Kim,⁴⁵ S. K. Kim,⁴³ Y. I. Kim,²¹ Y. J. Kim,⁶ K. Kinoshita,³
 S. Korpar,^{24,17} Y. Kozakai,²⁶ P. Križan,^{23,17} P. Krokovny,¹⁰ R. Kumar,³⁷ E. Kurihara,²
 Y. Kuroki,³⁶ A. Kuzmin,¹ Y.-J. Kwon,⁵⁷ S.-H. Kyeong,⁵⁷ J. S. Lange,⁵ G. Leder,¹⁴
 J. Lee,⁴³ J. S. Lee,⁴⁵ M. J. Lee,⁴³ S. E. Lee,⁴³ T. Lesiak,³¹ J. Li,⁹ A. Limosani,²⁵
 S.-W. Lin,³⁰ C. Liu,⁴² Y. Liu,⁶ D. Liventsev,¹⁶ J. MacNaughton,¹⁰ F. Mandl,¹⁴
 D. Marlow,³⁹ T. Matsumura,²⁶ A. Matyja,³¹ S. McOnie,⁴⁶ T. Medvedeva,¹⁶ Y. Mikami,⁵⁰
 K. Miyabayashi,²⁷ H. Miyata,³³ Y. Miyazaki,²⁶ R. Mizuk,¹⁶ G. R. Moloney,²⁵ T. Mori,²⁶
 T. Nagamine,⁵⁰ Y. Nagasaka,¹¹ Y. Nakahama,⁵¹ I. Nakamura,¹⁰ E. Nakano,³⁵ M. Nakao,¹⁰
 H. Nakayama,⁵¹ H. Nakazawa,²⁸ Z. Natkaniec,³¹ K. Neichi,⁴⁹ S. Nishida,¹⁰ K. Nishimura,⁹
 Y. Nishio,²⁶ I. Nishizawa,⁵³ O. Nitoh,⁵⁴ S. Noguchi,²⁷ T. Nozaki,¹⁰ A. Ogawa,⁴⁰ S. Ogawa,⁴⁸
 T. Ohshima,²⁶ S. Okuno,¹⁸ S. L. Olsen,^{9,13} S. Ono,⁵² W. Ostrowicz,³¹ H. Ozaki,¹⁰
 P. Pakhlov,¹⁶ G. Pakhlova,¹⁶ H. Palka,³¹ C. W. Park,⁴⁵ H. Park,²¹ H. K. Park,²¹
 K. S. Park,⁴⁵ N. Parslow,⁴⁶ L. S. Peak,⁴⁶ M. Pernicka,¹⁴ R. Pestotnik,¹⁷ M. Peters,⁹
 L. E. Pilonen,⁵⁶ A. Poluektov,¹ J. Rorie,⁹ M. Rozanska,³¹ H. Sahoo,⁹ Y. Sakai,¹⁰
 N. Sasao,²⁰ K. Sayeed,³ T. Schietinger,²² O. Schneider,²² P. Schönmeier,⁵⁰ J. Schümann,¹⁰
 C. Schwanda,¹⁴ A. J. Schwartz,³ R. Seidl,^{12,40} A. Sekiya,²⁷ K. Senyo,²⁶ M. E. Sevir,²⁵
 L. Shang,¹³ M. Shapkin,¹⁵ V. Shebalin,¹ C. P. Shen,⁹ H. Shibuya,⁴⁸ S. Shinomiya,³⁶
 J.-G. Shiu,³⁰ B. Shwartz,¹ V. Sidorov,¹ J. B. Singh,³⁷ A. Sokolov,¹⁵ A. Somov,³ S. Stanič,³⁴
 M. Starič,¹⁷ J. Stypula,³¹ A. Sugiyama,⁴¹ K. Sumisawa,¹⁰ T. Sumiyoshi,⁵³ S. Suzuki,⁴¹
 S. Y. Suzuki,¹⁰ O. Tajima,¹⁰ F. Takasaki,¹⁰ K. Tamai,¹⁰ N. Tamura,³³ M. Tanaka,¹⁰
 N. Taniguchi,²⁰ G. N. Taylor,²⁵ Y. Teramoto,³⁵ I. Tikhomirov,¹⁶ K. Trabelsi,¹⁰
 Y. F. Tse,²⁵ T. Tsuboyama,¹⁰ Y. Uchida,⁶ S. Uehara,¹⁰ Y. Ueki,⁵³ K. Ueno,³⁰
 T. Uglov,¹⁶ Y. Unno,⁸ S. Uno,¹⁰ P. Urquijo,²⁵ Y. Ushiroda,¹⁰ Y. Usov,¹ G. Varner,⁹

K. E. Varvell,⁴⁶ K. Vervink,²² S. Villa,²² A. Vinokurova,¹ C. C. Wang,³⁰ C. H. Wang,²⁹
J. Wang,³⁸ M.-Z. Wang,³⁰ P. Wang,¹³ X. L. Wang,¹³ M. Watanabe,³³ Y. Watanabe,¹⁸
R. Wedd,²⁵ J.-T. Wei,³⁰ J. Wicht,¹⁰ L. Widhalm,¹⁴ J. Wiechczynski,³¹ E. Won,¹⁹
B. D. Yabsley,⁴⁶ A. Yamaguchi,⁵⁰ H. Yamamoto,⁵⁰ M. Yamaoka,²⁶ Y. Yamashita,³²
M. Yamauchi,¹⁰ C. Z. Yuan,¹³ Y. Yusa,⁵⁶ C. C. Zhang,¹³ L. M. Zhang,⁴² Z. P. Zhang,⁴²
V. Zhilich,¹ V. Zhulanov,¹ T. Zivko,¹⁷ A. Zupanc,¹⁷ N. Zwahlen,²² and O. Zyukova¹

(The Belle Collaboration)

¹*Budker Institute of Nuclear Physics, Novosibirsk*

²*Chiba University, Chiba*

³*University of Cincinnati, Cincinnati, Ohio 45221*

⁴*Department of Physics, Fu Jen Catholic University, Taipei*

⁵*Justus-Liebig-Universität Gießen, Gießen*

⁶*The Graduate University for Advanced Studies, Hayama*

⁷*Gyeongsang National University, Chinju*

⁸*Hanyang University, Seoul*

⁹*University of Hawaii, Honolulu, Hawaii 96822*

¹⁰*High Energy Accelerator Research Organization (KEK), Tsukuba*

¹¹*Hiroshima Institute of Technology, Hiroshima*

¹²*University of Illinois at Urbana-Champaign, Urbana, Illinois 61801*

¹³*Institute of High Energy Physics,*

Chinese Academy of Sciences, Beijing

¹⁴*Institute of High Energy Physics, Vienna*

¹⁵*Institute of High Energy Physics, Protvino*

¹⁶*Institute for Theoretical and Experimental Physics, Moscow*

¹⁷*J. Stefan Institute, Ljubljana*

¹⁸*Kanagawa University, Yokohama*

¹⁹*Korea University, Seoul*

²⁰*Kyoto University, Kyoto*

²¹*Kyungpook National University, Taegu*

²²*École Polytechnique Fédérale de Lausanne (EPFL), Lausanne*

²³*Faculty of Mathematics and Physics, University of Ljubljana, Ljubljana*

²⁴*University of Maribor, Maribor*

²⁵*University of Melbourne, School of Physics, Victoria 3010*

²⁶*Nagoya University, Nagoya*

²⁷*Nara Women's University, Nara*

²⁸*National Central University, Chung-li*

²⁹*National United University, Miao Li*

³⁰*Department of Physics, National Taiwan University, Taipei*

³¹*H. Niewodniczanski Institute of Nuclear Physics, Krakow*

³²*Nippon Dental University, Niigata*

³³*Niigata University, Niigata*

³⁴*University of Nova Gorica, Nova Gorica*

³⁵*Osaka City University, Osaka*

³⁶*Osaka University, Osaka*

³⁷*Panjab University, Chandigarh*

³⁸*Peking University, Beijing*

- ³⁹*Princeton University, Princeton, New Jersey 08544*
⁴⁰*RIKEN BNL Research Center, Upton, New York 11973*
⁴¹*Saga University, Saga*
⁴²*University of Science and Technology of China, Hefei*
⁴³*Seoul National University, Seoul*
⁴⁴*Shinshu University, Nagano*
⁴⁵*Sungkyunkwan University, Suwon*
⁴⁶*University of Sydney, Sydney, New South Wales*
⁴⁷*Tata Institute of Fundamental Research, Mumbai*
⁴⁸*Toho University, Funabashi*
⁴⁹*Tohoku Gakuin University, Tagajo*
⁵⁰*Tohoku University, Sendai*
⁵¹*Department of Physics, University of Tokyo, Tokyo*
⁵²*Tokyo Institute of Technology, Tokyo*
⁵³*Tokyo Metropolitan University, Tokyo*
⁵⁴*Tokyo University of Agriculture and Technology, Tokyo*
⁵⁵*Toyama National College of Maritime Technology, Toyama*
⁵⁶*Virginia Polytechnic Institute and State University, Blacksburg, Virginia 24061*
⁵⁷*Yonsei University, Seoul*

Abstract

This paper describes a determination of the Cabibbo-Kobayashi-Maskawa matrix element $|V_{cb}|$ using the decay $B^0 \rightarrow D^{*-} \ell^+ \nu_\ell$. We perform a combined measurement of this quantity and of the form factors ρ^2 , $R_1(1)$, and $R_2(1)$ which fully characterize this decay in the framework of heavy-quark effective theory, based on 140 fb^{-1} of Belle data collected near the $\Upsilon(4S)$ resonance. The results, based on about 69,000 reconstructed $B^0 \rightarrow D^{*-} \ell^+ \nu_\ell$ decays, are $\rho^2 = 1.293 \pm 0.045 \pm 0.029$, $R_1(1) = 1.495 \pm 0.050 \pm 0.062$, $R_2(1) = 0.844 \pm 0.034 \pm 0.019$ and $\mathcal{F}(1)|V_{cb}| = 34.4 \pm 0.2 \pm 1.0$. The $B^0 \rightarrow D^{*-} \ell^+ \nu_\ell$ branching fraction is found to be $(4.42 \pm 0.03 \pm 0.25)\%$. For all these numbers, the first error is the statistical and the second is the systematic uncertainty. All results are preliminary.

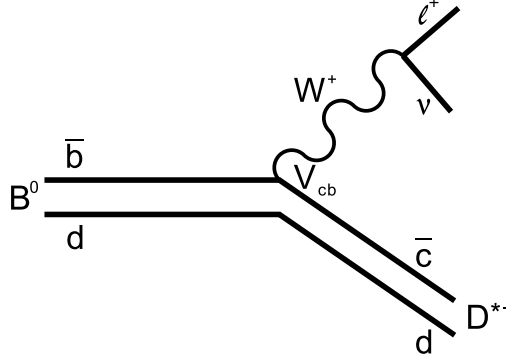


FIG. 1: Quark-level Feynman diagram for the decay $B^0 \rightarrow D^{*-} \ell^+ \nu_\ell$.

I. INTRODUCTION

The study of the decay $B^0 \rightarrow D^{*-} \ell^+ \nu_\ell$ is an important item on the B physics agenda for many reasons. First, the total rate is proportional to the magnitude of the Cabibbo-Kobayashi-Maskawa (CKM) matrix element V_{cb} [1] squared. We can thus determine this quantity from the measurement of this decay. Second, $B^0 \rightarrow D^{*-} \ell^+ \nu_\ell$ is a major background for charmless semileptonic B decays or semileptonic B decays with large missing energy. A precise knowledge of the form factors of this decay will thus help reducing systematic uncertainties in these analyses.

Our analysis technique follows closely previous studies of this decay using $e^+e^- \rightarrow \Upsilon(4S)$ data [2, 3, 4], *i.e.*, we reconstruct the D^* meson and the charged lepton only, without making any requirement on the other B meson in the event. The main difference to earlier analyses [2, 3] is that we measure the CKM matrix element and all three HQET form factors of this decay simultaneously. Also, by using a novel reconstruction technique of the B meson 4-momentum, we achieve a better resolution in the kinematic variables describing the $B^0 \rightarrow D^{*-} \ell^+ \nu_\ell$ decay, which translates into an improved determination of the HQET form factors.

II. THEORETICAL FRAMEWORK

A. Kinematic variables

The decay $B^0 \rightarrow D^{*-} \ell^+ \nu_\ell$ [5] proceeds chiefly through the tree-level transition shown in Fig. 1. Its kinematics can be fully characterized by four variables:

The first one is w , defined by

$$w = \frac{p_B \cdot p_{D^*}}{m_B m_{D^*}} = \frac{m_B^2 + m_{D^*}^2 - q^2}{2m_B m_{D^*}}, \quad (1)$$

where m_B and m_{D^*} are the masses of the B and the D^* mesons (5.2794 GeV and 2.010 GeV, respectively [6]), p_B and p_{D^*} are their four-momenta, and $q^2 = (p_\ell + p_\nu)^2$. In the B rest frame, approximately equal to the $\Upsilon(4S)$ center-of-mass (c.m.) frame, the expression for w reduces to the Lorentz boost $\gamma_{D^*} = E_{D^*}/m_{D^*}$. The ranges of w and q^2 are restricted by the

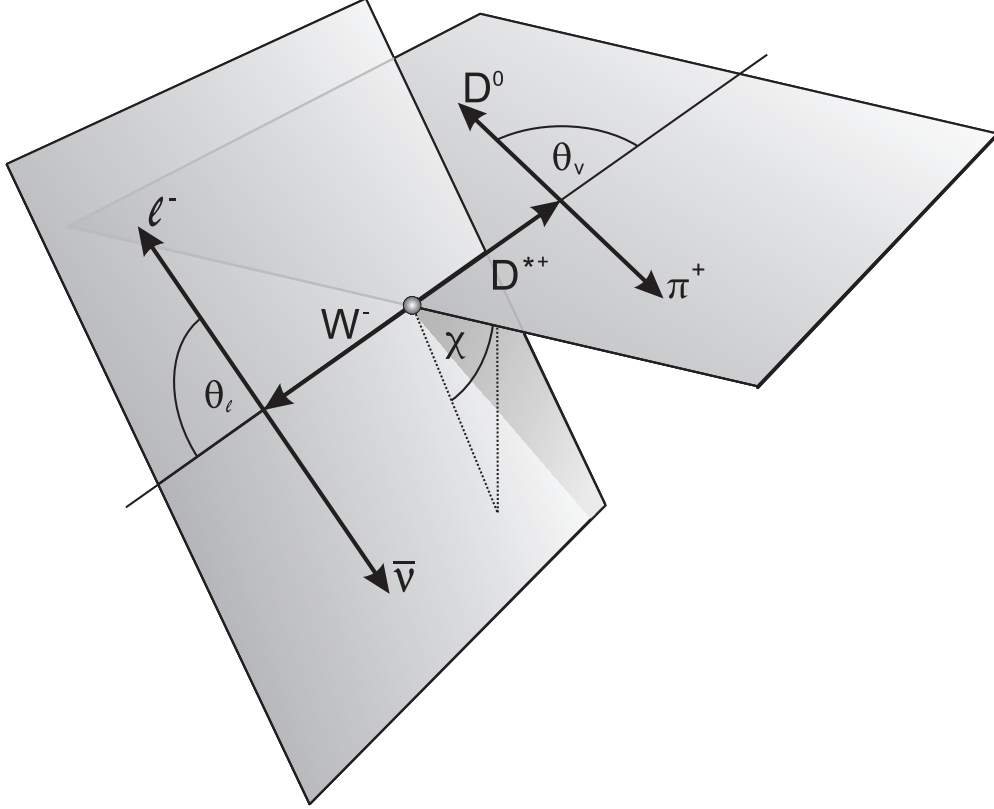


FIG. 2: Definition of the angles θ_ℓ , θ_V and χ for the decay $B^0 \rightarrow D^{*-} \ell^+ \nu_\ell$, $D^{*-} \rightarrow \bar{D}^0 \pi_s^-$.

kinematics of the decay, with $q^2 = 0$ corresponding to

$$w_{\max} = \frac{m_B^2 + m_{D^*}^2}{2m_B m_{D^*}} \approx 1.504, \quad (2)$$

and $w_{\min} = 1$ to

$$q_{\max}^2 = (m_B - m_{D^*})^2 = 10.69 \text{ GeV}^2. \quad (3)$$

The point $w = 1$ is also referred to as zero recoil.

The remaining three variables are the angles shown in Fig. 2:

- θ_ℓ , the angle between the direction of the lepton in the virtual W rest frame and the direction of the W in the B rest frame;
- θ_V , the angle between the direction of the D meson in the D^* rest frame and the direction of the D^* meson in the B rest frame;
- χ , the angle between the D^* and W decay planes in the B rest frame.

B. Four-dimensional decay distribution

The Lorentz structure of the $B^0 \rightarrow D^{*-} \ell^+ \nu_\ell$ decay amplitude can be expressed in terms of three helicity amplitudes (H_+ , H_- , and H_0), which correspond to the three polarization

states of the D^* , two transverse and one longitudinal. For low-mass leptons (electrons and muons), these amplitudes are expressed in terms of the three functions $h_{A_1}(w)$, $R_1(w)$, and $R_2(w)$ [7]

$$H_i(w) = m_B \frac{R^*(1-r^2)(w+1)}{2\sqrt{1-2wr+r^2}} h_{A_1}(w) \tilde{H}_i(w), \quad (4)$$

where

$$\tilde{H}_{\mp} = \frac{\sqrt{1-2wr+r^2} \left(1 \pm \sqrt{\frac{w-1}{w+1}} R_1(w)\right)}{1-r}, \quad (5)$$

$$\tilde{H}_0 = 1 + \frac{(w-1)(1-R_2(w))}{1-r}, \quad (6)$$

with $R^* = (2\sqrt{m_B m_{D^*}})/(m_B + m_{D^*})$ and $r = m_{D^*}/m_B$. The functions $R_1(w)$ and $R_2(w)$ are defined in terms of the axial and vector form factors as,

$$A_2(w) = \frac{R_2(w)}{R^{*2}} \frac{2}{w+1} A_1(w), \quad (7)$$

$$V(w) = \frac{R_1(w)}{R^{*2}} \frac{2}{w+1} A_1(w). \quad (8)$$

By convention, the function $h_{A_1}(w)$ is defined as

$$h_{A_1}(w) = \frac{1}{R^*} \frac{2}{w+1} A_1(w). \quad (9)$$

For $w \rightarrow 1$, the axial form factor $A_1(w)$ dominates, and in the limit of infinite b - and c -quark masses, a single form factor describes the decay, the so-called Isgur-Wise function [8, 9].

The fully differential decay rate in terms of the three helicity amplitudes is [10]

$$\begin{aligned} \frac{d^4\Gamma(B^0 \rightarrow D^{*-}\ell^+\nu_\ell)}{dw d(\cos\theta_\ell) d(\cos\theta_V) d\chi} &= \frac{6m_B m_{D^*}^2}{8(4\pi)^4} \sqrt{w^2-1} (1-2wr+r^2) G_F^2 |V_{cb}|^2 \\ &\times \left\{ (1-\cos\theta_\ell)^2 \sin^2\theta_V H_+^2(w) + (1+\cos\theta_\ell)^2 \sin^2\theta_V H_-^2(w) \right. \\ &+ 4\sin^2\theta_\ell \cos^2\theta_V H_0^2(w) - 2\sin^2\theta_\ell \sin^2\theta_V \cos 2\chi H_+(w) H_-(w) \\ &- 4\sin\theta_\ell (1-\cos\theta_\ell) \sin\theta_V \cos\theta_V \cos\chi H_+(w) H_0(w) \\ &\left. + 4\sin\theta_\ell (1+\cos\theta_\ell) \sin\theta_V \cos\theta_V \cos\chi H_-(w) H_0(w) \right\}, \end{aligned} \quad (10)$$

with $G_F = (1.16637 \pm 0.00001) \times 10^{-5} \text{ GeV}^{-2}$. By integrating this decay rate over all but one of the four variables, w , $\cos\theta_\ell$, $\cos\theta_V$, or χ , we obtain the four one-dimensional decay distributions from which we will extract the form factors. The differential decay rate as a function of w is

$$\frac{d\Gamma}{dw} = \frac{G_F^2}{48\pi^3} m_{D^*}^3 (m_B - m_{D^*})^2 \mathcal{G}(w) \mathcal{F}^2(w) |V_{cb}|^2, \quad (11)$$

where

$$\begin{aligned} \mathcal{F}^2(w) \mathcal{G}(w) &= h_{A_1}^2(w) \sqrt{w-1} (w+1)^2 \left\{ 2 \left[\frac{1-2wr+r^2}{(1-r)^2} \right] \right. \\ &\times \left[1 + R_1(w)^2 \frac{w-1}{w+1} \right] + \left[1 + (1-R_2(w)) \frac{w-1}{1-r} \right]^2 \left. \right\}, \end{aligned}$$

and $\mathcal{G}(w)$ is a known phase space factor,

$$\mathcal{G}(w) = \sqrt{w^2 - 1}(w + 1)^2 \left[1 + 4 \frac{w}{w + 1} \frac{1 - 2wr + r^2}{(1 - r)^2} \right].$$

In the infinite quark-mass limit, the heavy quark symmetry (HQS) predicts $\mathcal{F}(1) = 1$. Corrections to this limit have been calculated in lattice QCD. A calculation, performed in the quenched approximation, predicts (including a QED correction of 0.7%) $\mathcal{F}(1) = 0.919^{+0.030}_{-0.035}$ [11]. This value is compatible with estimates based on non-lattice methods [12]. A recent unquenched lattice result, $\mathcal{F}(1) = 0.930 \pm 0.022$, is still preliminary [13].

C. Form factor parameterization

The heavy quark effective theory (HQET) allows to obtain a parameterization of these form-factors. Perfect heavy quark symmetry implies that $R_1(w) = R_2(w) = 1$, *i.e.*, the form factors A_2 and V are identical for all values of w and differ from A_1 only by a simple kinematic factor. Corrections to this approximation have been calculated in powers of Λ_{QCD}/m_b and the strong coupling constant α_s . Various parameterizations in powers of $(w - 1)$ have been proposed. Among the different predictions relating the coefficients of the higher order terms to the linear term, we adopt the following expressions derived by Caprini, Lellouch and Neubert [14],

$$h_{A_1}(w) = h_{A_1}(1) [1 - 8\rho^2 z + (53\rho^2 - 15)z^2 - (231\rho^2 - 91)z^3], \quad (12)$$

$$R_1(w) = R_1(1) - 0.12(w - 1) + 0.05(w - 1)^2, \quad (13)$$

$$R_2(w) = R_2(1) + 0.11(w - 1) - 0.06(w - 1)^2, \quad (14)$$

where $z = (\sqrt{w + 1} - \sqrt{2})/(\sqrt{w + 1} + \sqrt{2})$. The three parameters ρ^2 , $R_1(1)$, and $R_2(1)$, cannot be calculated; they must be extracted from data.

III. EXPERIMENTAL PROCEDURE

A. Data sample and event selection

The data used in this analysis were taken with the Belle detector [15] at the KEKB asymmetric energy e^+e^- collider [16]. Belle is a large-solid-angle magnetic spectrometer that consists of a three-layer silicon vertex detector, a 50-layer central drift chamber (CDC), an array of aerogel threshold Cherenkov counters (ACC), a barrel-like arrangement of time-of-flight scintillation counters (TOF), and an electromagnetic calorimeter (ECL) comprised of CsI(Tl) crystals located inside a super-conducting solenoid coil that provides a 1.5 T magnetic field. An iron flux-return located outside of the coil is instrumented to detect K_L^0 mesons and to identify muons (KLM).

The data sample consists of 140 fb^{-1} taken at the $\Upsilon(4S)$ resonance, or 152×10^6 $B\bar{B}$ events. Another 15 fb^{-1} taken at 60 MeV below the resonance are used to estimate the non- $B\bar{B}$ (continuum) background. The off-resonance data is scaled by the integrated on- to off-resonance luminosity ratio corrected for the $1/s$ dependence of the $q\bar{q}$ cross-section.

Generic Monte Carlo samples equivalent to about three times the integrated luminosity are used in this analysis. Monte Carlo simulated events are generated with the `evtgen` program [17] and full detector simulation based on `GEANT` [18] is applied. QED bremsstrahlung in $B \rightarrow X\ell\nu$ decays is added using the `PHOTOS` package [19].

Hadronic events are selected based on the charged track multiplicity and the visible energy in the calorimeter. The selection is described in detail elsewhere [20]. We also apply a moderate cut on the ratio of the second to the zeroth Fox-Wolfram moment [21], $R_2 < 0.4$, to reject continuum events.

B. Event reconstruction

Charged tracks are required to originate from the interaction point by applying the following selections on the impact parameters in $r\phi$ and z , $|dr| < 2$ cm and $|dz| < 4$ cm, respectively. Additionally, we demand at least one associated hit in the SVD detector. For pion and kaon candidates, the Cherenkov light yield from ACC, the time-of-flight information from TOF and dE/dx from CDC are required to be consistent with the respective mass hypothesis.

Neutral D meson candidates are searched for in the decays channels $D^0 \rightarrow K^-\pi^+$ and $D^0 \rightarrow K^-\pi^+\pi^-\pi^+$. We fit the charged tracks to a common vertex and reject the D^0 candidate if the χ^2 -probability is below 10^{-3} . The momenta of the charged tracks are re-evaluated at the vertex and the D^0 4-momentum is calculated as their sum. The reconstructed D^0 mass is required to lie within ± 3 standard deviations from m_{D^0} , where one sigma is about 4.5 MeV (4 MeV) for the one (three) pion mode.

The D^0 candidate is combined with a slow pion π_s^+ (appropriately charged with respect to the kaon candidate) to form a D^{*+} candidate. No impact parameter and SVD hit requirements are applied for π_s . Again, a vertex fit is performed and the same vertex requirement is applied. The invariant mass difference between the D^* and the D candidates, Δm , is required to lie within 144 and 147 MeV. Additional continuum suppression is achieved by requiring a D^* momentum below 2.45 GeV in the c.m. frame.

Finally, the D^* candidate is combined with an oppositely charged lepton (electron or muon). Electron candidates are identified using the ratio of the energy detected in the ECL to the track momentum, the ECL shower shape, position matching between track and ECL cluster, the energy loss in the CDC and the response of the ACC counters. Muons are identified based on their penetration range and transverse scattering in the KLM detector. In the momentum region relevant to this analysis, charged leptons are identified with an efficiency of about 90% and the probability to misidentify a pion as an electron (muon) is 0.25% (1.4%) [22, 23]. No SVD hit requirement is made for lepton tracks. In the lab frame, the (transverse) momentum of the lepton is required to exceed 0.85 GeV/ c (0.6 GeV/ c). We also apply an upper lepton momentum cut at 2.4 GeV in the c.m. frame to reject continuum. Again, a vertex fit is performed and $D^{*+}\ell^-$ candidates are rejected if the vertex probability is less than 10^{-3} .

Figures 3 and 4 show the invariant mass of the D^0 candidates and the Δm distributions, respectively.

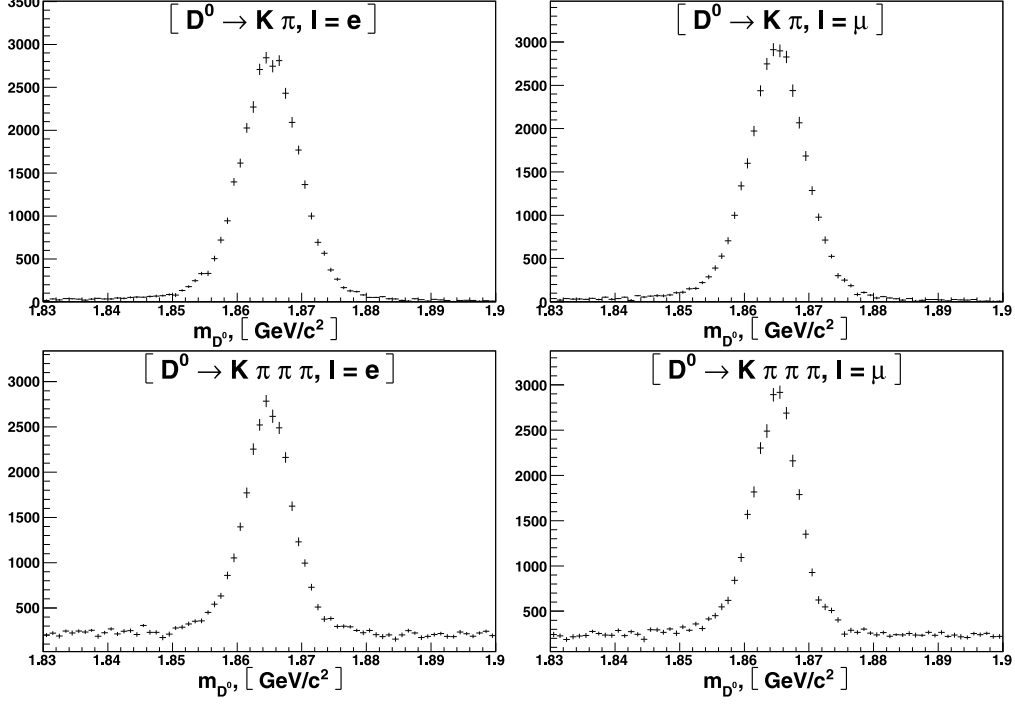


FIG. 3: Invariant D^0 candidate mass distributions in the different sub-samples. All analysis cuts (except on the plotted variable) and $|\cos \theta_{B,D^*\ell}| < 1$ are applied.

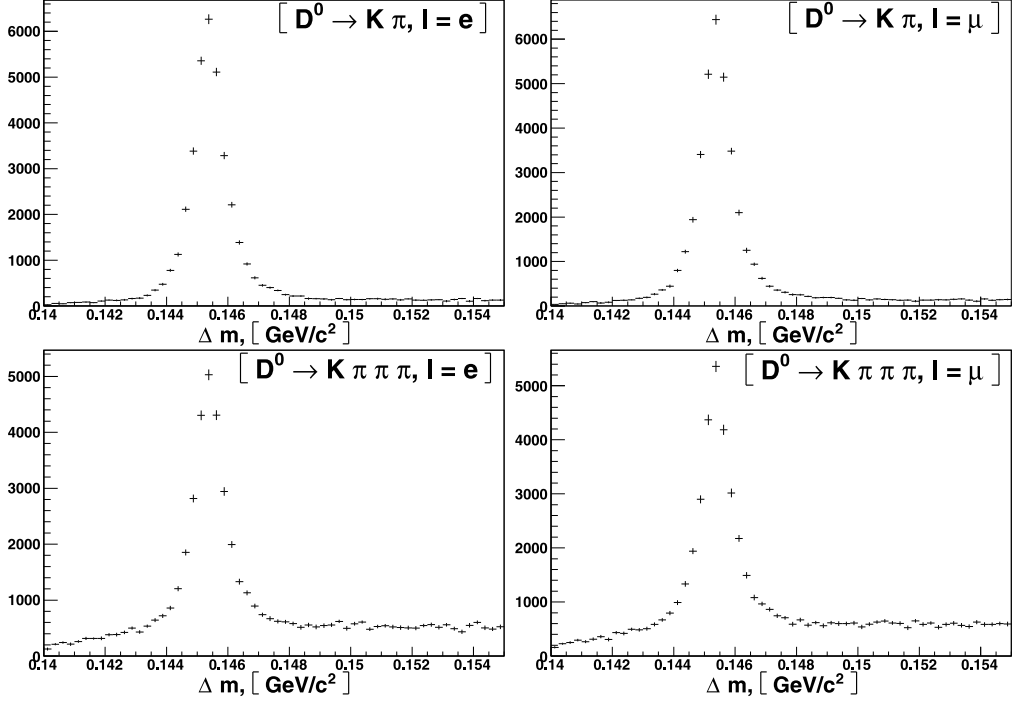


FIG. 4: Δm distributions in the different sub-samples. All analysis cuts (except on the plotted variable) and $|\cos \theta_{B,D^*\ell}| < 1$ are applied.

C. Background estimation

Because we do not reconstruct the other B meson in the event, the B momentum is *a priori* unknown. However, in the c.m. frame, one can show that the B direction lies on a cone around the $(D^*\ell)$ -axis [24],

$$\cos \theta_{B,D^*\ell} = \frac{2E_B^*E_{D^*\ell}^* - m_B^2 - m_{D^*\ell}^2}{2|\vec{p}_B^*||\vec{p}_{D^*\ell}^*|}, \quad (15)$$

where E_B^* is half of the c.m. energy and $|\vec{p}_B^*|$ is $\sqrt{E_B^{*2} - m_B^2}$. The quantities $E_{D^*\ell}^*$, $\vec{p}_{D^*\ell}^*$ and $m_{D^*\ell}$ are calculated from the reconstructed $D^*\ell$ system.

This cosine is also a powerful discriminator between signal and background: Signal events should strictly lie in the interval $(-1, 1)$, although – due to finite detector resolution – about 8% of the signal is reconstructed outside this interval. The background on the other hand does not have this restriction. We therefore perform a fit to the $\cos \theta_{B,D^*\ell}$ distribution to determine the background normalizations from the data.

The background contained in the selected events can be attributed to the following six sources:

- continuum: any candidate reconstructed in a non- $\Upsilon(4S)$ event
- fake lepton: the charged lepton candidate is fake; the D^* candidate might be fake or not
- fake D^* : the D^* candidate is misreconstructed; the lepton candidate is an actual electron or muon
- D^{**} : background from $B \rightarrow \bar{D}^{**}\ell^+\nu$ decays with $\bar{D}^{**} \rightarrow D^{*-}\pi$ or $B \rightarrow D^{*-}\pi\ell^+\nu$ non-resonant
- correlated background: background from other processes in which the D^* and the lepton stem from the same B meson, *e.g.* $B^0 \rightarrow D^{*-}\tau^+\nu$, $\tau^+ \rightarrow \mu^+\nu\nu$
- uncorrelated background: the D^* and the lepton stem from different B mesons

These background components are modeled by $(D^*\ell)$ -candidates, appropriately selected from MC data based on generator information, except continuum which is modeled by off-resonance events. The shape of the fake muon background is corrected by the ratio of the pion fake rate in the experimental data over the same quantity in the MC simulation, as measured using kinematically identified pions in $K_S^0 \rightarrow \pi^+\pi^-$ decays. The $\cos \theta_{B,D^*\ell}$ distribution in the data is fitted using the `TFractionFitter` algorithm [25] in `ROOT` [26]. The fit is done separately in the four sub-samples defined by the D^0 decay channel and the lepton type. The results are shown in Fig. 5 and Table I.

In all fits, the continuum normalization is fixed to the on- to off-resonance luminosity ratio, corrected for the $1/s$ dependence of the $e^+e^- \rightarrow q\bar{q}$ cross-section. The normalizations of some other components have also been fixed to the MC expectations if their contributions cannot be determined reliably from the $\cos \theta_{B,D^*\ell}$ spectrum, as indicated in the table. In general, the normalizations obtained by the fit agree well with the MC expectations except for the D^{**} component which is too abundant in the MC.

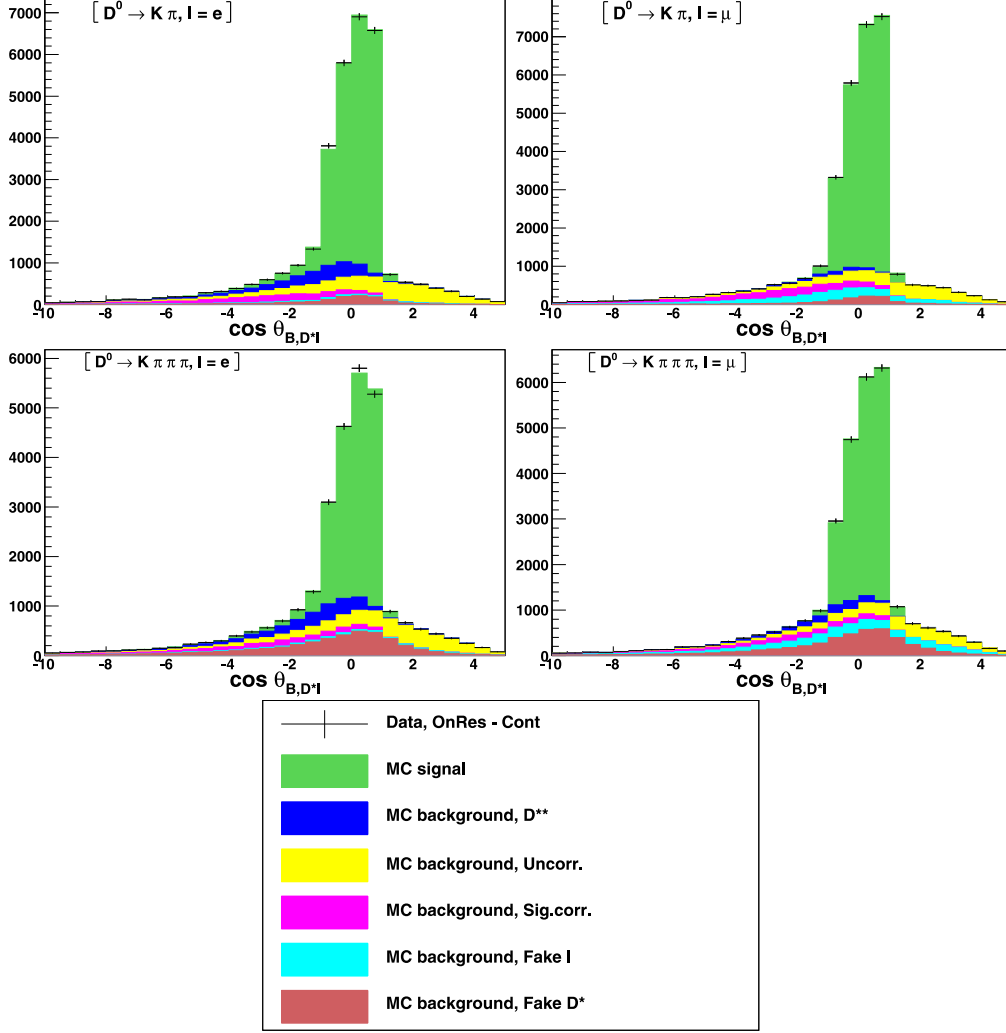


FIG. 5: Result of the fits to the $\cos \theta_{B,D^* \ell}$ distributions in the different sub-samples.

sample	$K\pi, e$	$K\pi, \mu$	$K3\pi, e$	$K3\pi, \mu$
signal	$(80.95 \pm 1.06)\%$	$(80.92 \pm 0.98)\%$	$(73.17 \pm 1.71)\%$	$(72.22 \pm 1.46)\%$
D^{**}	$(4.73 \pm 0.87)\%$	$(1.24 \pm 0.85)\%$	$(5.21 \pm 1.18)\%$	$(2.85 \pm 1.10)\%$
uncorrelated	$(5.36 \pm 0.27)\%$	$(4.38 \pm 0.29)\%$	$(5.42 \pm 0.58)\%$	$(4.17 \pm 0.54)\%$
correlated	$(1.69 \pm 0.26)\%$	$(2.42 \pm 0.28)\%$	$(2.04 \pm 0.69)\%$	$(2.25 \pm 0.59)\%$
fake ℓ	0.68% (fixed)	3.62% (fixed)	0.72% (fixed)	4.04% (fixed)
fake D^*	2.96% (fixed)	2.91% (fixed)	$(8.78 \pm 2.63)\%$	$(9.63 \pm 2.15)\%$
continuum	3.62% (fixed)	4.51% (fixed)	4.81% (fixed)	4.87% (fixed)

TABLE I: The signal and background fractions for selected events within the signal window $|\cos \theta_{B,D^* \ell}| < 1$.

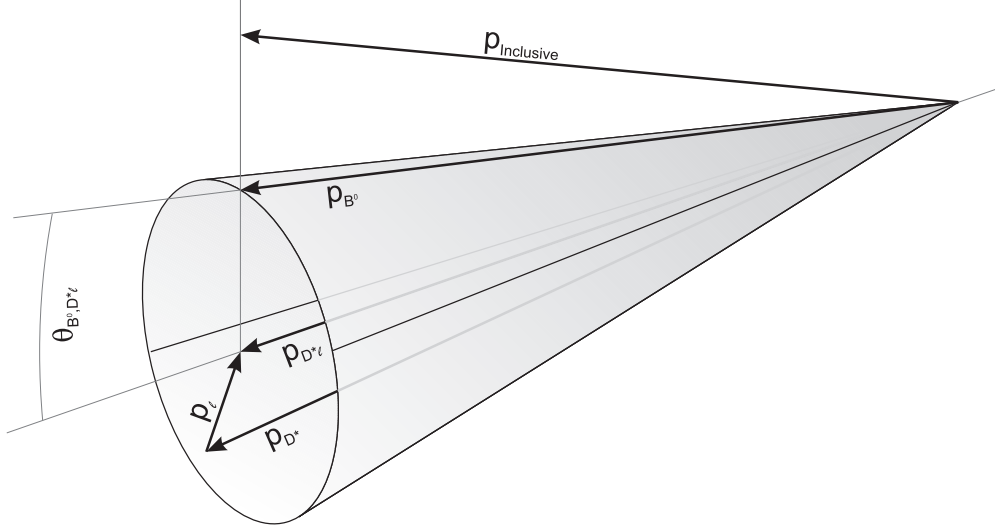


FIG. 6: Reconstruction of the B^0 direction. Refer to the text for details.

D. Kinematic variables

To calculate the four kinematic variables – w , $\cos\theta_\ell$, $\cos\theta_V$ and χ – that characterize the $B^0 \rightarrow D^{*-}l^+\nu$ decay defined in Sect. II A, we need to determine the B^0 rest frame. The B direction is already known to be on a cone around the $(D^*\ell)$ -axis with opening angle $2\theta_{B,D^*\ell}$ in the c.m. frame, Eq. (15). For the best guess of the B direction, we first estimate the c.m. frame B vector by summing the momenta of the remaining particles in the event ($\vec{p}_{\text{inclusive}}^*$ [24]) and choose the direction on the cone that minimizes the difference to $\vec{p}_{\text{inclusive}}^*$, as shown in Fig. 6.

To obtain $\vec{p}_{\text{inclusive}}^*$, we exclude tracks passing very far away from the interaction point or compatible with a multiply reconstructed track generated by a low-momentum particle spiraling in the central drift chamber. Unmatched clusters in the barrel region must have an energy greater than 50 MeV. For clusters in the forward (backward) region, the threshold is at 100 MeV (150 MeV). Then, we compute $\vec{p}_{\text{inclusive}}$ (in the lab. frame) by summing the 3-momenta of the selected particles,

$$\vec{p}_{\text{inclusive}} = \vec{p}_{\text{HER}} + \vec{p}_{\text{LER}} - \sum_i \vec{p}_i, \quad (16)$$

where the indices HER and LER correspond to the colliding beams, and transform this vector into the c.m. frame. Note that we do not make any mass assumption for the charged particles. The energy component of $p_{\text{inclusive}}$ is defined by requiring $E_{\text{inclusive}}^*$ to be $E_{\text{beam}}^* = \sqrt{s}/2$.

With the B^0 rest frame reconstructed in this way, the resolutions in the kinematic variables are found to be about 0.025, 0.052, 0.047 and 6.47° for w , $\cos\theta_\ell$, $\cos\theta_V$ and χ , respectively.

E. Fit procedure

In the rest of this analysis, we consider only events passing the signal window requirement $|\cos\theta_{B,D^*\ell}| < 1$. We perform a binned χ^2 fit of the w , $\cos\theta_\ell$, $\cos\theta_V$ and χ distributions

over (almost) the entire phase space to measure the following quantities: the form factor normalization $\mathcal{F}(1)|V_{cb}|$ Eq. (11), and the three parameters ρ^2 , $R_1(1)$ and $R_2(1)$ which parameterize the form factor in the HQET framework Eqs. (12)–(14). Instead of fitting in four dimensions, we fit simultaneously the one-dimensional projections of w , $\cos\theta_\ell$, $\cos\theta_V$ and χ to have enough entries in each bin of the fit. This introduces bin-to-bin correlations which have to be accounted for.

The distributions in w , $\cos\theta_\ell$, $\cos\theta_V$ and χ are divided into ten bins of equal width. The kinematically allowed values of w are between 1 and ≈ 1.504 but we restrict the w range to values between 1 and 1.5. In each sub-sample, there are thus 40 bins to be used in the fit. In the following, we label these bins with a common index i , $i = 1, \dots, 40$, *i.e.*, depending on the value of i , the i^{th} bin might belong to the w , $\cos\theta_\ell$, $\cos\theta_V$ or χ distribution.

The predicted number of events N_i^{th} in the bin i is given by

$$N_i^{\text{th}} = N_{B^0} \mathcal{B}(D^{*+} \rightarrow D^0 \pi^+) \mathcal{B}(D^0) \tau_{B^0} \Gamma_i, \quad (17)$$

where N_{B^0} is the number of B^0 mesons in the data sample and $\mathcal{B}(D^{*+} \rightarrow D^0 \pi^+)$ is taken from Ref. [6]. In the $(K\pi, e)$ and $(K\pi, \mu)$ sub-samples $\mathcal{B}(D^0)$ is $\mathcal{B}(D^0 \rightarrow K^- \pi^+)$ [6]; in $(K3\pi, e)$ and $(K3\pi, \mu)$ $\mathcal{B}(D^0)$ is $R_{K3\pi/K\pi} \mathcal{B}(D^0 \rightarrow K^- \pi^+)$, with $R_{K3\pi/K\pi}$ a fifth free parameter of the fit. Finally, τ_{B^0} is the B^0 lifetime [6], and Γ_i is the width obtained by integrating Eq. (10) in the kinematic variable corresponding to i from the lower to the upper bin boundary (the other kinematic variables are integrated over their full range). This integration is numerical in the case of w and analytic for the other variables. The expected number of events N_i^{exp} is related to N_i^{th} as follows

$$N_i^{\text{exp}} = \sum_{j=1}^{40} (R_{ij} \epsilon_j N_j^{\text{th}}) + N_i^{\text{bkg}}. \quad (18)$$

Here, ϵ_i is the probability that an event generated in the bin i is reconstructed and passes all analysis cuts, and R_{ij} is the detector response matrix, *i.e.*, it gives the probability that an event generated in the bin j is observed in the bin i . Both quantities are calculated using MC simulation. N_i^{bkg} is the number of expected background events, estimated as described in Sect. III C.

Next, we calculate the variance σ_i^2 of N_i^{exp} . We consider the following contributions: the uncertainty in N_i^{th} (poissonian); fluctuations related to N repetitions of the yes/no experiment with known success probability ϵ_i (binomial); a similar contribution to the variance related to R_{ij} (multinomial); and the uncertainty in the background contribution N_i^{bkg} . This yields the following expression for σ_i^2 ,

$$\begin{aligned} \sigma_i^2 = \sum_{j=1}^{40} \left[R_{ij}^2 \epsilon_j^2 N_j^{\text{th}} + R_{ij}^2 \frac{\epsilon_j(1-\epsilon_j)}{N_{\text{data}}} (N_j^{\text{th}})^2 + \frac{R_{ij}(1-R_{ij})}{N'_{\text{data}}} \epsilon_j^2 (N_j^{\text{th}})^2 + \right. \\ \left. R_{ij}^2 \frac{\epsilon_j(1-\epsilon_j)}{N_{\text{MC}}} (N_j^{\text{th}})^2 + \frac{R_{ij}(1-R_{ij})}{N'_{\text{MC}}} \epsilon_j^2 (N_j^{\text{th}})^2 \right] + \sigma^2(N_i^{\text{bkg}}). \end{aligned} \quad (19)$$

The first term is the poissonian uncertainty in N_i^{th} . The second and third terms are the binomial and multinomial uncertainties related to the finite real data size, respectively, where N_{data} (N'_{data}) is the total number of decays (the number of reconstructed decays) into the final state under consideration ($K\pi$ or $K3\pi$, e or μ) in the real data. The quantities ϵ_i and

R_{ij} are calculated from a finite signal MC sample (N_{MC} and N'_{MC}); the corresponding uncertainties are estimated by the fourth and fifth terms. Finally, the last term is the background contribution $\sigma^2(N_i^{\text{bkg}})$, calculated as the sum of the different background component variances. For each background component defined in Sect. III C we estimate its contribution by linear error propagation of the scale factor and the error determined by the procedure described above. For continuum, we estimate the error in the on-resonance to off-resonance luminosity ratio to be 1.5%.

In each sub-sample, we calculate the off-diagonal elements of the covariance matrix cov_{ij} as $Np_{ij} - Np_i p_j$, where p_{ij} is the relative abundance of the bin (i, j) in the 2-dimensional histogram obtained by plotting the kinematic variables against each other, p_i is the relative number of entries in the 1-dimensional distribution, and N is the size of the sample. Covariances are calculated for the signal and the different background components, and added with appropriate normalizations.

The covariance matrix is inverted numerically within ROOT and, labelling the four sub-samples ($K\pi$ or $K3\pi$, e or μ) with the index k , the sub-sample χ^2 functions are calculated,

$$\chi_k^2 = \sum_{i,j} (N_i^{\text{obs}} - N_i^{\text{exp}}) C_{ij}^{-1} (N_j^{\text{obs}} - N_j^{\text{exp}}), \quad (20)$$

where N_i^{obs} is the number of events observed in bin i in the data. We sum these four functions and minimize the global χ^2 with MINUIT [27].

We have tested this fit procedure using generic MC data samples. All results are consistent with expectations and show no indication of bias.

IV. RESULTS AND SYSTEMATIC UNCERTAINTIES

A. Results

After applying all selection requirements and subtracting backgrounds, $69,345 \pm 377$ signal events are found in the data. The preliminary result of the fit to these events is shown in Fig. 7 and Table II. The statistical correlation coefficients of the five fit parameters are given in Table III.

As explained earlier, the branching fraction for the decay $D^0 \rightarrow K^- \pi^+ \pi^+ \pi^-$ is floated in the fit to the full sample. The fit result is compatible with the recent measurement by the CLEO-c experiment [28]. In the sub-sample fits, $R_{K3\pi/K\pi}$ is fixed to the value of the full sample fit.

B. Systematic uncertainties

To estimate the systematic uncertainties in the results quoted above, we consider contributions from the following sources: uncertainties in the background component normalizations, uncertainty in the MC tracking efficiency, errors in $\mathcal{B}(D^{*+} \rightarrow D^0 \pi^+)$ and $\mathcal{B}(D^0 \rightarrow K^- \pi^+)$ [6], and uncertainties in the B^0 lifetime [6] and the total number of B^0 mesons in the data sample.

To estimate the uncertainty related to a given background component, we vary the normalization by ± 1 standard deviation of the fit described in Sect. III C. The uncertainty in

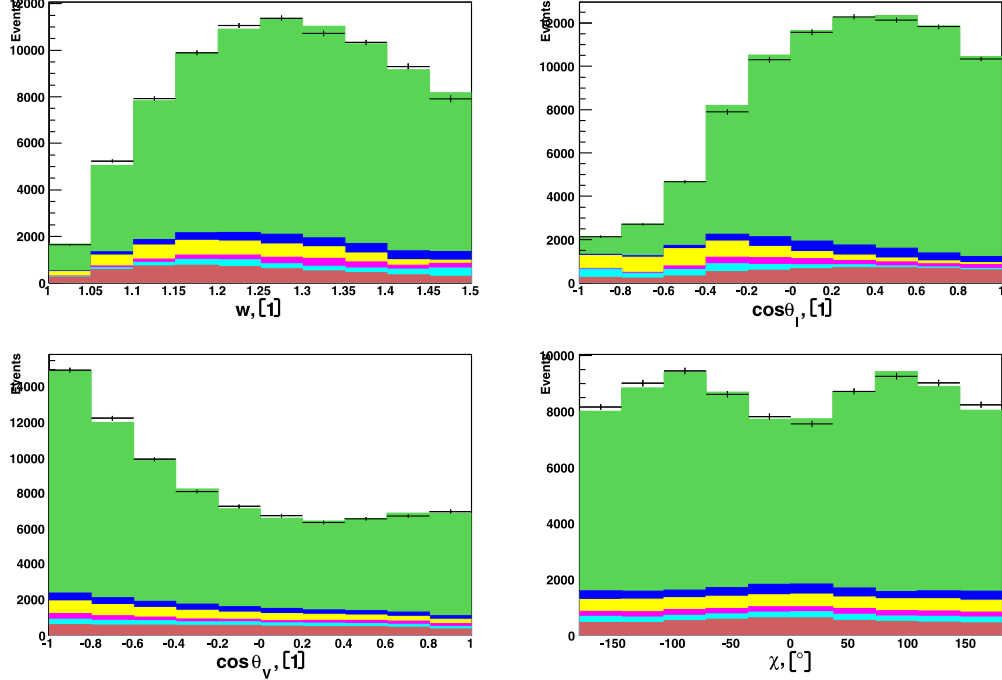


FIG. 7: Preliminary result of the fit of the four kinematic variables in the total sample. (The different sub-samples are added in this plot.) The points with error bars are continuum subtracted on-resonance data. The histograms are the signal and the different background components. The color scheme is explained in Fig. 5.

the $D^{**}\ell\nu$ component is inflated by a factor of two to make the amount of $D^{**}\ell\nu$ in each sub-sample consistent. The error in the continuum normalization is taken to be 1.5% as explained earlier.

For the tracking uncertainty, we calculate the track finding error considering only the D^0 decay into $K^-\pi^+$, as the branching fraction for $D^0 \rightarrow K^-\pi^+\pi^-\pi^+$ is fitted from data. (A possible mismodeling of the tracking efficiency for this mode would be absorbed in $R_{K3\pi/K\pi}$.) We thus have four charged tracks. Assuming 1% uncertainty for each track, except for the slow pion from D^{*+} for which we use 2%, and adding these uncertainties linearly, we obtain a tracking uncertainty of 5%. Given the size of this error, the uncertainty in the lepton identification (1–2%) can be neglected.

The breakup of the systematic error quoted in Table II is given in Table IV.

V. SUMMARY AND DISCUSSION

We have reconstructed about 69,000 $B^0 \rightarrow D^{*-}\ell^+\nu_\ell$ decays using a 140 fb^{-1} data sample recorded at the $\Upsilon(4S)$ resonance with the Belle detector at the KEKB accelerator. A fit to four kinematic variables fully characterizing this decays yields to measurements of the form factor normalization $\mathcal{F}(1)|V_{cb}|$ and of the parameters ρ^2 , $R_1(1)$ and $R_2(1)$ that enter the HQET form factor parameterization of this decay. We obtain: $\mathcal{F}(1)|V_{cb}| = 34.4 \pm 0.2 \pm 1.0$, $\rho^2 = 1.293 \pm 0.045 \pm 0.029$, $R_1(1) = 1.495 \pm 0.050 \pm 0.062$, $R_2(1) = 0.844 \pm 0.034 \pm 0.019$, and $\mathcal{B}(B^0 \rightarrow D^{*-}\ell^+\nu_\ell) = (4.42 \pm 0.03 \pm 0.25)\%$. For all these numbers, the first error is the

sample	$K\pi, e$	$K\pi, \mu$	$K3\pi, e$
ρ^2	$1.329 \pm 0.072 \pm 0.017$	$1.221 \pm 0.075 \pm 0.046$	$1.238 \pm 0.233 \pm 0.053$
$R_1(1)$	$1.455 \pm 0.077 \pm 0.046$	$1.608 \pm 0.087 \pm 0.099$	$1.085 \pm 0.125 \pm 0.044$
$R_2(1)$	$0.782 \pm 0.055 \pm 0.014$	$0.853 \pm 0.055 \pm 0.027$	$0.980 \pm 0.087 \pm 0.027$
$R_{K3\pi/K\pi}$	2.153 (fixed)	2.153 (fixed)	2.153 (fixed)
$\mathcal{B}(B^0 \rightarrow D^{*-}\ell^+\nu_\ell)$ (%)	$4.43 \pm 0.03 \pm 0.25$	$4.41 \pm 0.03 \pm 0.26$	$4.42 \pm 0.04 \pm 0.25$
$\mathcal{F}(1) V_{cb} $ (10^{-3})	$34.3 \pm 0.4 \pm 1.0$	$33.5 \pm 0.4 \pm 1.0$	$35.6 \pm 0.8 \pm 1.3$
$\chi^2/\text{n.d.f.}$	29.2/36	37.4/36	19.2/36
$P(\chi^2)$	78.2%	40.4%	99.0%

sample	$K3\pi, \mu$	average	full sample
ρ^2	$1.436 \pm 0.121 \pm 0.062$	1.299 ± 0.045	$1.293 \pm 0.045 \pm 0.029$
$R_1(1)$	$1.643 \pm 0.163 \pm 0.112$	1.427 ± 0.050	$1.495 \pm 0.050 \pm 0.062$
$R_2(1)$	$0.842 \pm 0.105 \pm 0.038$	0.844 ± 0.034	$0.844 \pm 0.034 \pm 0.019$
$R_{K3\pi/K\pi}$	2.153 (fixed)		2.153 ± 0.011
$\mathcal{B}(B^0 \rightarrow D^{*-}\ell^+\nu_\ell)$ (%)	$4.47 \pm 0.04 \pm 0.26$	4.43 ± 0.02	$4.42 \pm 0.03 \pm 0.25$
$\mathcal{F}(1) V_{cb} $ (10^{-3})	$35.6 \pm 0.7 \pm 1.3$	34.5 ± 0.2	$34.4 \pm 0.2 \pm 1.0$
$\chi^2/\text{n.d.f.}$	17.9/36		138.8/155
$P(\chi^2)$	99.5%		82.0%

TABLE II: The results of the fits to the sub-samples, their average and the fit result on the total sample. The first error is statistical, the second is the estimated systematic uncertainty. The breakup of the systematic uncertainty is given in Table III. All numbers are preliminary.

	$\mathcal{F}(1) V_{cb} $	ρ^2	$R_1(1)$	$R_2(1)$	$R_{K3\pi/K\pi}$
$\mathcal{F}(1) V_{cb} $	1.000	0.635	-0.285	-0.220	0.011
ρ^2		1.000	0.388	-0.870	0.040
$R_1(1)$			1.000	-0.511	0.001
$R_2(1)$				1.000	0.002
$R_{K3\pi/K\pi}$					1.000

TABLE III: The statistical correlation coefficients of the five parameters in the fit to the full sample.

statistical and the second is the systematic uncertainty. These results are compatible with the recent BaBar measurements of these quantities [4]. All numbers are preliminary.

Acknowledgments

We thank the KEKB group for the excellent operation of the accelerator, the KEK cryogenics group for the efficient operation of the solenoid, and the KEK computer group and the National Institute of Informatics for valuable computing and SINET3 network support.

	ρ^2	$R_1(1)$	$R_2(1)$	$\mathcal{B}(D^*\ell\nu_\ell)$	$\mathcal{F}(1) V_{cb} $
D^{**}	0.015	0.038	0.011	0.051	0.25
uncorrelated	0.009	0.028	0.002	0.003	0.04
correlated	0.003	0.003	0.007	0.028	0.14
fake ℓ	0.020	0.037	0.009	0.002	0.04
fake D^*	0.012	0.011	0.009	0.034	0.33
continuum	0.003	0.008	0.000	0.001	0.02
tracking	–	–	–	0.221	0.86
$\mathcal{B}(D^0 \rightarrow K^-\pi^+)$ [6]	–	–	–	0.081	0.31
$\mathcal{B}(D^{*+} \rightarrow D^0\pi^+)$ [6]	–	–	–	0.033	0.13
$\tau(B^0)$ [6]	–	–	–	0.026	0.10
$N(B\bar{B})$	–	–	–	0.036	0.14
f_{+-}/f_{00} [6]	0.003	0.011	0.005	0.001	0.04
total	0.029	0.062	0.019	0.251	1.04

TABLE IV: The breakup of the systematic uncertainty in the result of the fit to the full sample.

We acknowledge support from the Ministry of Education, Culture, Sports, Science, and Technology of Japan and the Japan Society for the Promotion of Science; the Australian Research Council and the Australian Department of Education, Science and Training; the National Natural Science Foundation of China under contract No. 10575109 and 10775142; the Department of Science and Technology of India; the BK21 program of the Ministry of Education of Korea, the CHEP SRC program and Basic Research program (grant No. R01-2005-000-10089-0) of the Korea Science and Engineering Foundation, and the Pure Basic Research Group program of the Korea Research Foundation; the Polish State Committee for Scientific Research; the Ministry of Education and Science of the Russian Federation and the Russian Federal Agency for Atomic Energy; the Slovenian Research Agency; the Swiss National Science Foundation; the National Science Council and the Ministry of Education of Taiwan; and the U.S. Department of Energy.

-
- [1] N. Cabibbo, Phys. Rev. Lett. **10**, 531 (1963);
M. Kobayashi and T. Maskawa, Prog. Theor. Phys. **49**, 652 (1973).
 - [2] R. A. Briere *et al.* [CLEO Collaboration], Phys. Rev. Lett. **89**, 081803 (2002) [arXiv:hep-ex/0203032].
 - [3] K. Abe *et al.* [BELLE Collaboration], Phys. Lett. B **526**, 247 (2002) [arXiv:hep-ex/0111060].
 - [4] B. Aubert *et al.* [BABAR Collaboration], Phys. Rev. D **77**, 032002 (2008) [arXiv:0705.4008 [hep-ex]].
 - [5] Throughout this note charge conjugation is implied.
 - [6] W. M. Yao *et al.* [Particle Data Group], J. Phys. G **33**, 1 (2006).
 - [7] M. Neubert, Phys. Rept. **245**, 259 (1994) [arXiv:hep-ph/9306320].
 - [8] N. Isgur and M. B. Wise, Phys. Lett. B **232**, 113 (1989).

- [9] N. Isgur and M. B. Wise, Phys. Lett. B **237**, 527 (1990).
- [10] J. D. Richman and P. R. Burchat, Rev. Mod. Phys. **67**, 893 (1995) [arXiv:hep-ph/9508250].
- [11] S. Hashimoto, A. S. Kronfeld, P. B. Mackenzie, S. M. Ryan and J. N. Simone, Phys. Rev. D **66**, 014503 (2002) [arXiv:hep-ph/0110253].
- [12] N. Uraltsev, arXiv:hep-ph/0010328.
- [13] J. Laiho [Fermilab Lattice and MILC Collaborations], PoS **LATTICE2007**, 358 (2007) [arXiv:0710.1111 [hep-lat]].
- [14] I. Caprini, L. Lellouch and M. Neubert, Nucl. Phys. B **530**, 153 (1998) [arXiv:hep-ph/9712417].
- [15] A. Abashian *et al.* [Belle Collaboration], Nucl. Instrum. Meth. A **479**, 117 (2002).
- [16] S. Kurokawa, Nucl. Instrum. Meth. A **499**, 1 (2003), and other papers included in this volume.
- [17] D. J. Lange, Nucl. Instrum. Meth. A **462**, 152 (2001).
- [18] R. Brun, F. Bruyant, M. Maire, A. C. McPherson and P. Zanarini, CERN-DD/EE/84-1.
- [19] E. Barberio and Z. Was, Comput. Phys. Commun. **79**, 291 (1994).
- [20] K. Abe *et al.* [Belle Collaboration], Phys. Rev. D **64**, 072001 (2001) [hep-ex/0103041].
- [21] G. C. Fox and S. Wolfram, Phys. Rev. Lett. **41**, 1581 (1978).
- [22] K. Hanagaki, H. Kakuno, H. Ikeda, T. Iijima and T. Tsukamoto, Nucl. Instrum. Meth. A **485**, 490 (2002) [hep-ex/0108044].
- [23] A. Abashian *et al.*, Nucl. Instrum. Meth. A **491**, 69 (2002).
- [24] Quantities evaluated in the c.m. frame are denoted by an asterisk.
- [25] R. J. Barlow and C. Beeston, Comput. Phys. Commun. **77**, 219 (1993).
- [26] R. Brun and F. Rademakers, Nucl. Instrum. Meth. A **389** (1997) 81.
- [27] F. James and M. Roos, Comput. Phys. Commun. **10**, 343 (1975).
- [28] Q. He *et al.* [CLEO Collaboration], Phys. Rev. Lett. **95**, 121801 (2005) [Erratum-ibid. **96**, 199903 (2006)] [arXiv:hep-ex/0504003].